land

MDPI

Article

Intensity Analysis for Urban Land Use/Land Cover Dynamics Characterization of Ouagadougou and Bobo-Dioulasso in Burkina Faso

Valentin Ouedraogo [1,*], Kwame Oppong Hackman [2], Michael Thiel [3] and Jaiye Dukiya [4]

[1] West African Science Service Centre on Climate Change and Adapted Land Use (WASCAL), Doctoral Research Programme on Climate Change and Human Habitat, Federal University of Technology, P.M.B 65, Minna 920101, Niger State, Nigeria
[2] West African Science Service Centre on Climate Change and Adapted Land Use (WASCAL), Competence Centre, Ouagadougou 06 BP 9507, Burkina Faso; hackman.k@wascal.org
[3] Department of Remote Sensing, Institute of Geography and Geology, Julius-Maximilians-University of Würzburg, Oswald-Külpe-Weg 86, 97074 Würzburg, Germany; michael.thiel@uni-wuerzburg.de
[4] Department of Urban and Regional Planning, Federal University of Technology, P.M.B 65, Minna 920101, Niger State, Nigeria; duksat2000@futminna.edu.ng
* Correspondence: valentinoued@gmail.com or ouedraogo.v@edu.wascal.org; Tel.: +226-73-434-230

Abstract: Ouagadougou and Bobo-Dioulasso remain the two major urban centers in Burkina Faso with an increasing trend in human footprint. The research aimed at analyzing the Land Use/Land Cover (LULC) dynamics in the two cities between 2003 and 2021 using intensity analysis, which decomposes LULC changes into interval, category and transition levels. The satellite data used for this research were composed of surface reflectance imagery from Landsat 5, Landsat 7 and Landsat 8 acquired from the Google Earth Engine Data Catalogue. The Random Forest, Support Vector Machine and Gradient Tree Boost algorithms were employed to run supervised image classifications for four selected years including 2003, 2009, 2015 and 2021. The results showed that the landscape is changing in both cities due to rapid urbanization. Ouagadougou experienced more rapid changes than Bobo-Dioulasso, with a maximum annual change intensity of 3.61% recorded between 2015 and 2021 against 2.22% in Bobo-Dioulasso for the period 2009–2015. The transition of change was mainly towards built-up areas, which gain targeted bare and agricultural lands in both cities. This situation has led to a 78.12% increase of built-up surfaces in Ouagadougou, while 42.24% of agricultural land area was lost. However, in Bobo-Dioulasso, the built class has increased far more by 140.67%, and the agricultural land areas experienced a gain of 1.38% compared with the 2003 baseline. The study demonstrates that the human footprint is increasing in both cities making the inhabitants vulnerable to environmental threats such as flooding and the effect of an Urban Heat Island, which is information that could serve as guide for sustainable urban land use planning.

Keywords: Land Use/Land Cover; urbanization; intensity analysis; Google Earth Engine

Citation: Ouedraogo, V.; Hackman, K.O.; Thiel, M.; Dukiya, J. Intensity Analysis for Urban Land Use/Land Cover Dynamics Characterization of Ouagadougou and Bobo-Dioulasso in Burkina Faso. *Land* **2023**, *12*, 1063. https://doi.org/10.3390/land12051063

Academic Editor: Jianjun Zhang

Received: 15 April 2023
Revised: 5 May 2023
Accepted: 9 May 2023
Published: 13 May 2023

1. Introduction

Urbanization refers to the massive movement of population to urban settings and the consequent spatial and demographic growths that occur in urban areas [1]. In 2018, the United Nations estimated that about 4.2 billion people were living in urban areas [2]. By the year 2050, the world's total urban population will reach 6.7 billion, while about 0.6 to 1.3 million square kilometers of land will be converted into urban areas [3]. In Africa, the rate of urbanization is arguably the highest in the world [4] and is projected to reach 55% of the total population by 2050 [5]. The rapid trend of urbanization in Africa has been confirmed by several authors [4–7] and is characterized by the increasing number of its megacities, cities and towns [5]. The urban growth in most of the developing countries, over the past two decades, has been unprecedented due to the population growth and the global

technological transformation and political change [8]. Being key economic centers in terms of production and consumption, the cities in developing countries lack capacities to deliver relevant goods and services to their citizens. In Burkina Faso for example, the urbanization process is inconsistent with the local plans and policies, resulting in the formation of slums where socio-economic facilities such as transportation, water and sanitation, health and education are lacking [9].

Rapid urbanization is making the planning of sustainable urban development problematic [10], because the demand for land is increasing together with unplanned development. The consequence of increasing land demand in urban areas is the spatial and temporal modification of Land Use/Land Cover (LULC) [11] towards built surfaces at the expense of natural areas. Thus, the urban LULC changes affect the thermal characteristics of the surface [12] and expose cities to climate change from greenhouse gas-induced radiative forcing and localized effects such as Urban Heat Island (UHI) [13]. Thus, LULC changes contribute to global climate change [14] and lead to landscape and ecosystem degradation [15]. It is well known that natural land cover such as vegetated and water body areas release water vapor into the atmosphere and contribute to urban environmental cooling, while impervious surfaces (i.e., built-up areas, pavements, and asphalt) modify the drainage geography, intensify runoff and increase the risk of flooding [16].

In Burkina Faso, the combined effects of the natural growth of population and positive net migration [17] have placed Ouagadougou and Bobo-Dioulasso in a continuous urban expansion process [18]. The increase in population generates a high demand on land for housing and agro-businesses development, creating LULC fragmentation within the inner city and the development of new built areas at the peripheral zones. This situation, in addition to the unprecedented land speculation occurring in the area, particularly in Ouagadougou [19], leads to a spatial urban expansion characterized by the development of informal housing and consequently an increase of impervious surfaces at the expense of natural vegetation and water bodies. In Ouagadougou for instance, because of the increasing trend of informal housing in the urban fringe, some former rural areas have been swallowed up by urban restructuration processes [20]. The urbanization process causes the transformation of permeable surfaces into impervious surfaces including concrete and asphalt, which decrease the soil infiltration capacity and increase runoff and flood flows as well [21]. So, systematic LULC mapping is necessary to understand and monitor the changes in the urban landscape to facilitate sustainable urban development planning.

Although few studies have been carried out on urban LULC mapping [22–24], most of them used individual classification algorithms results to show the landscape changes. The use of multi-temporal images taking into consideration the variation in spectral reflectance of the surface material implies the combination of large number of images, which require more processing time and storage. In addition, the application of a method involving the use of majority voting of multiple machine learning classifiers results is also storage demanding. Thankfully in recent years, LULC studies using satellite data are becoming easy due to the operationalisation of cloud-computing platforms such as Google Earth Engine (GEE), a geo-computational cloud platform where users can access relevant long-term big geodata and processing tools for environmental monitoring without any need for downloading and storing in local systems [25–27]. In the African region, GEE has been employed to map LULC either for urban growth assessment and monitoring [6], ecosystem degradation assessment [28] or ecological monitoring [29].

In the study area, not only was a LULC mapping using GEE not found, but also the application of intensity analysis, which shows insights to the patterns of changes in order to relate it to the causal processes [30], is yet to be explored. The aim of this study is to map the spatio-temporal pattern of LULC in Ouagadougou and Bobo-Dioulasso using multi-temporal satellite images in the GEE environment, characterizing the changes by means of intensity analysis framework.

2. Materials and Methods

2.1. Study Area Description

The study was conducted in Ouagadougou and Bobo-Dioulasso, the first two largest cities of Burkina Faso. Ouagadougou is located in the Centre Region between longitudes 1°41′31″ W and 1°21′05″ W and between latitudes 12°12′42″ N and 12°30′14″ N, while Bobo-Dioulasso is situated in the Hauts-Bassins Region between longitudes 4°23′40″ W and 4°12′19″ W and between latitudes 11°06′26″ N and 11°17′27″ N (Figure 1). Ouagadougou covers an area of 970 km^2 while Bobo-Dioulasso's land mass is 1779 km^2. Ouagadougou lies in the so-called Central peneplain of Burkina Faso, with altitudes varying between 272 and 368 meters above sea level, while the relief in Bobo-Dioulasso ranges between 287 and 558 metres above sea level.

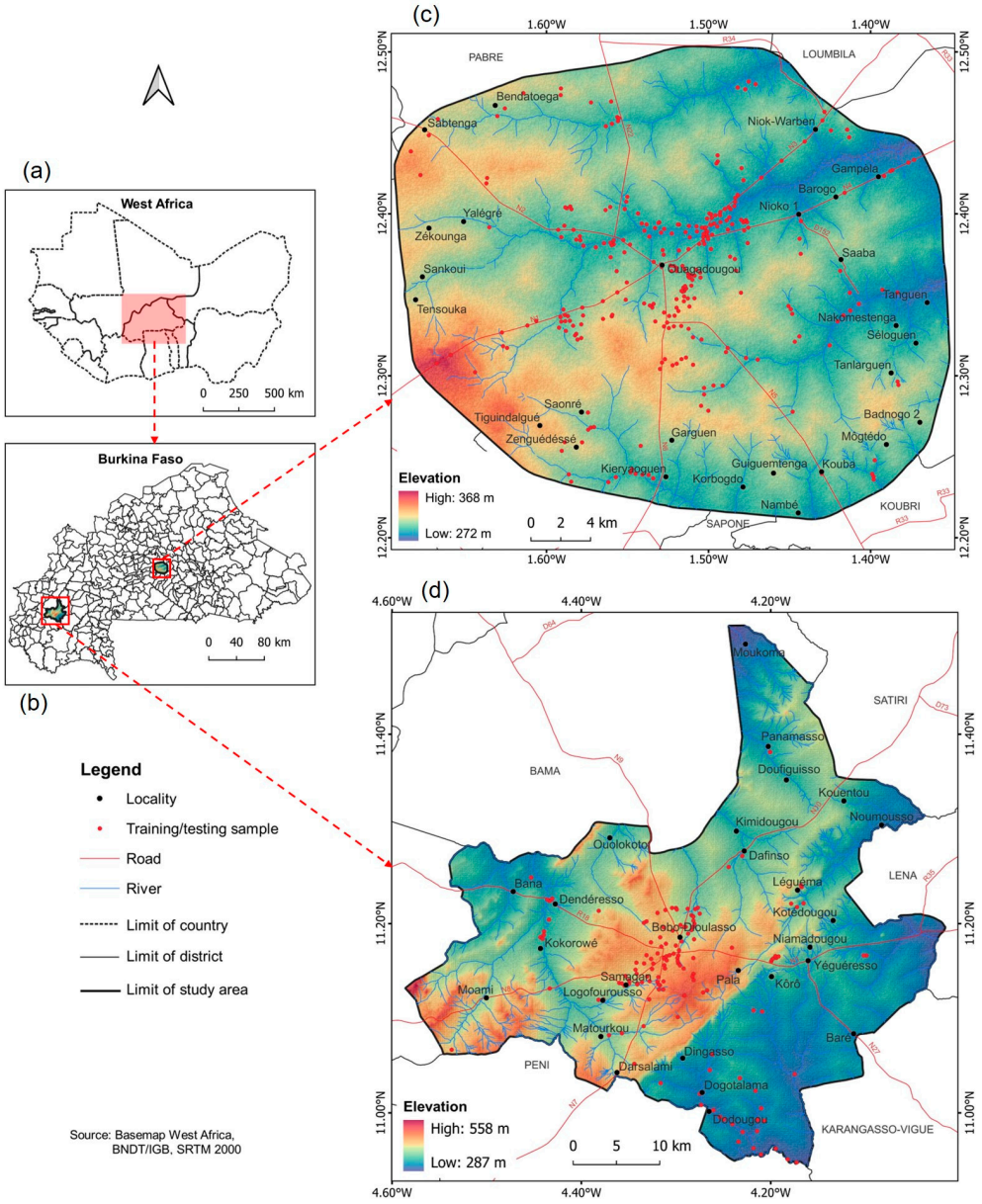

Figure 1. Location of study area. (**a**) West Africa inset Burkina Faso; (**b**) Burkina Faso showing administrative boundaries of districts inset Ouagadougou and Bobo-Dioulasso in red boxes; (**c**) Zoom of Ouagadougou showing elevation, roads, rivers, localities and training/testing samples; (**d**) Zoom of Bobo-Dioulasso showing elevation, roads, rivers, localities and training/testing samples.

In terms of climate, both cities belong to the Sudanian climatic zone. Thus, similar to the whole of West Africa, the climate is regulated by the movement of the Inter-Tropical Convergence Zone (ITCZ). During the study period (2003–2021), the average monthly temperature varied between 25.2 °C and 33.3 °C in Ouagadougou and between 25.5 °C and 31.1 °C in Bobo-Dioulasso. The total annual rainfall ranged from 571 to 1003 mm/year in Ouagadougou, whereas in Bobo-Dioulasso, it ranged from 682 to 1370 mm/year. Ouagadougou and Bobo-Dioulasso, being the most developed cities of the country, have experienced a rapid spatial growth characterized by the expansion of built-up area to the detriment of natural land cover. The population of Ouagadougou evolved from 172,661 inhabitants in 1975 to 2,415,266 inhabitants in 2019 [17,31]. The population in Bobo-Dioulasso increased from 115,063 inhabitants in 1975 to 904,920 inhabitants in 2019 [17,31].

2.2. Satellite Data Acquisition and Pre-Processing

For this research, the GEE platform was used. It is a cloud-based geospatial analysis platform that provides easy and instant access to satellite data and computing resources to process them directly, without the need for downloading [26]. The satellite images for the LULC mapping were collected from Landsat 5 Thematic Mapper (TM), Landsat 7 Enhanced Thematic Mapper plus (ETM+) and Landsat 8 Operational Land Imager (OLI) sensors, provided by the United States Geological Survey (USGS). All the images used were surface reflectance data from the Level 2 Collection 2 Tier 1 datasets, which are second-generation Landsat pre-processed products. Prior to their ingestion into GEE Data Catalogue, the images were pre-processed to at-surface reflectance level using the Landsat Ecosystem Disturbance Adaptative Processing System (LEDAPS) algorithm in the case of Landsat 5 and 7 and the Landsat Surface Reflectance Code (LaSRC) in the case of Landsat 8 OLI [32]. To gather relevant images for the study, a search was made through the Landsat (5, 7 and 8) images, from 2003 to 2021, that cover Ouagadougou (Path 195, Row 051) and Bobo-Dioulasso (Path 197, Row 052 and Path 196, Row 052) metropolitan areas. For each year, the images from October to December were considered for the analyses to reduce the number of cloudy data and enhance the level of discrimination between the different classes. Additional pre-processing tasks including scaling and cloud masking were performed on the images. Regarding the scaling procedure, the scale factor and offset value provided in the bands description in GEE catalogue were used to reconstitute the surface reflectance values of the images. A cloud masking, using the Quality Assessment (QA) band, was also conducted on images with low cloud cover (<10%). Furthermore, the USGS Landsat 7 gap-filling method was employed to correct the spatial discontinuity in the images due to the Scan Line Corrector (SLC) failure in May 2003 which resulted on about 22% of data lost in each image scene [33].

2.3. Satellite Images Processing

For the LULC mapping, six atmospherically corrected surface reflectance bands, namely, Blue, Green, Red, Near-Infrared and Shortwave-Infrared band 1 (SWIR 1) and Shortwave-Infrared band 2 (SWIR 2), were used. Assuming that the land cover type and configuration remained the same in both rainy and dry seasons, the median image for the October–December period for each year was computed from the image collections obtained for each classification year. In addition to the spectral bands, additional inputs composed of topographic derivatives (elevation and slope), as well as vegetation and some land cover specific indices, were computed. The vegetation indices useful to discriminate vegetation from other LULC classes include the Normalized Difference Vegetation Index (NDVI) [6] and Enhanced Vegetation Index [34]. Dry Built-up Index (DBI), Dry Bare-soil Index (DBSI) and Normalized Difference Built-up Index (NDBI) [35], Bare Soil Index (BSI) and Soil Adjusted Vegetation Index (SAVI) [36] and Normalized Difference Water Index (NDWI) [11] were the biophysical indices used. SAVI is used to correct NDVI for the influence of soil brightness in areas with low vegetation cover. BSI is used to show the difference between agricultural and non-agricultural land thanks to its ability to detect

bare soil and fallow lands [36]. DBI and DBSI are used in combination with NDBI to help distinguish between built-up areas and bare lands, rather than using only NDBI due to its inability to distinguish between the two units in dry climate [35], as in the context of Burkina Faso. Furthermore, Principal Component Analysis (PCA), a statistical method that reduces the dimensionality of a large datasets, was performed on the median images to extract the main uncorrelated bands that contain most of the spectral information [37]. In sum, the predictors used for the image classification were composed of the median images, the vegetation and biophysical indices, the topographic elements including elevation and slope derived from the Shuttle Radar Topographic Mission (SRTM) Digital Elevation Model (DEM) image at a spatial resolution of 30 m and the three Principal Components (PC). Table 1 gives the description of the different predictors used for the Land Use/Land Cover classification.

Table 1. Details of the predictors used in the image classification (All predictors are calculated on a spatial resolution of 30 m. ρx represents the reflection in band x).

Predictor	Computation Equation	Description
med(Blue)	median from October to December	Median band of all blue bands in the period
med(Green)	median from October to December	Median band of all green bands in the period
med(Red)	median from October to December	Median band of all red bands in the period
med(NIR)	median from October to December	Median band of all NIR bands in the period
med(SWIR 1)	median from October to December	Median band of all SWIR1 bands in the period
med(SWIR 2)	median from October to December	Median band of all SWIR2 bands in the period
Elevation	Automatic	Elevation level
Slope	Automatic	Slope classes
PC1	PCA	First principal component
PC2	PCA	Second principal component
PC3	PCA	Third principal component
NDVI	$\frac{\rho_{NIR}-\rho_{RED}}{\rho_{NIR}+\rho_{RED}}$	Index to differentiate vegetation class from others
SAVI	$1.5 \times \frac{(\rho_{NIR}-\rho_{RED})}{(\rho_{NIR}+\rho_{RED}+0.5)}$	Index to account for soil noise
NDWI	$\frac{\rho_{Green}-\rho_{NIR}}{\rho_{Green}+\rho_{NIR}}$	Index to discriminate water class from others
NDBI	$\frac{\rho_{SWIR1}-\rho_{NIR}}{\rho_{SWIR1}+\rho_{NIR}}$	Index to distinguish built-up for other classes
DBI	$\frac{\rho_{BLUE}-\rho_{TIR}}{\rho_{BLUE}+\rho_{TIR}} - NDVI$	Index to differentiate built-up from bare land
DBSI	$\frac{\rho_{SWIR1}-\rho_{GREEN}}{\rho_{SWIR1}+\rho_{GREEN}} - NDVI$	Index to differentiate built-up from bare land

2.4. Land Use/Land Cover Classification Scheme

In total, four years were considered for the LULC analysis with a time step of six years: 2003, 2009, 2015 and 2021. The classification scheme used in this study is composed of five LULC classes including built-up, bare land, forest, agricultural land and water (Table 2). Agricultural areas were combined with shrub land to have agricultural land class. This is because of the fact that agricultural areas look like savannah parks in the case of cultivated areas or shrubs in the case of fallow lands. This similarity implies a spectral confusion between the two classes in the region. The class considered as bare land is composed of areas cleaned for construction or used for public activities such as football and meetings [6] and untarred roads.

Table 2. Description of LULC classes, adapted from [38,39].

LULC Classes	Description
Built-up	Area dominated by urban, peri-urban and rural settlements including pavement, tarred roads and other concrete surfaces
Bare land	Surfaces without vegetation, building or water and untarred roads
Forest	Area occupied by urban parks and forests
Agricultural land	Cultivated lands including seasonal, and permanent crops as well as fallows, shrubland and grassland
Water	Rivers, dams and lakes

2.5. Reference Samples Collection

The reference samples were collected, observing a minimum mapping unit of 30 × 30 metres of homogeneous landscape [34] to match the Landsat satellites images resolution (30 m). A point was then picked at the center of each homogenous unit. The collection was made on Google Earth Pro high-resolution images through on-screen digitization. For the purposes of quantitative analyses and comparison, consistent point samples were collected throughout the four years. Given that the area is in continuous urbanization and most of the Land Use/Land Cover classes are being transformed to built-up areas, a change logic was assumed to collect the samples. Thus, for the built-up class, the earliest image was used as reference, assuming that in urban areas the conversion from other classes to built-up is irreversible. Moreover, to ensure that the samples are consistent throughout the period, the "Show historical imagery" tool in Google Earth Pro (version 7.3.6.9345) was employed to move forward, year after year, in order to record the pixels that remained built-up from 2003 to 2021. For the other classes (water, forest, bare-land, and agricultural land), the latest image was used making sure that the class of each sample is the same throughout the time series by going back in time and retaining the consistent pixels for the analysis. In total, 289 and 144 homogeneous and consistent samples were collected in Ouagadougou and Bobo-Dioulasso, respectively. Ouagadougou has more samples than Bobo-Dioulasso because more cloud-free historical high-resolution images were found over this area. However, in Bobo-Dioulasso, only the central area (urban core) was covered by clear images.

2.6. Land Use/Land Cover Classification

The image classification was performed using machine learning algorithms. Then, the collected reference datasets were divided into training and testing set to avoid overfitting [40]. In general, the best results are obtained with 70–80% of the samples assigned to training sets and 20–30% of the data for testing sets [40]. For this study, 80% of the samples were used to train the model, and 20% were used for testing. A pixel-based image classification method was applied using three different supervised classifiers available in GEE: Random Forest (RF), Support Vector Machine (SVM) and Gradient Tree Boost (GTB). RF is an ensemble of classification trees which employs bagging operation to generate multiple decision trees (ntree) based on a randomly selected subset of training data. Each tree is then grown to its maximum size based on a bootstrapped sample from the training dataset without any pruning, and each node is split using the best among a subset of input variables (mtry) [41]. The classification is performed by using the most voted class from each tree predictor. SVM is a non-parametric supervised machine learning algorithm considering that for a nonlinear separable dataset, consisting of points from two classes, all the points of one class can be separated from those of the other class by using an infinite number of hyperplanes. The best hyperplane with the largest margin between the two classes is selected by using a subset of training samples known as support vectors [42]. RF and SVM have high performance in time-series image classification [43], achieving good accuracies in several studies conducted in the region [34,44–46]. The GTB is a gradient-boosting algorithm that uses regression trees as weak classifiers. The weak learners measure the error observed in each node, split the node and return the values [47].

2.7. Land Use/Land Cover Post-Classification Majority Filtering

In order to improve the final results, the LULC images from the different classifiers were converted to an image collection, and a vertical majority filtering (using the mode function) was performed to have a single classified image. To perform the image classification in GEE, numbers were assigned to each class (0: water, 1: Built-up, 2: Agricultural land, 3: Forest and 4: Bare land). Thus, the majority filtering process consisted of a spatial overlay of the outputs of the different classifiers after which, for each pixel, the most frequently occurring LULC class (the corresponding number) across the collection was selected as the final pixel label. In other words, the majority voting calculated the most common class

at each pixel level across the collection of classified images. When there is one majority vote (e.g., 1, 1, 3), the majority value is returned (the majority pixel value is 1). In case where there are multiple mode values (not applicable for this study, because it used three classifiers) or there is no majority vote (e.g., 2, 1, 5), the minimum pixel value is returned (the minimum value is 1). Naboureh et al. [48] found an improvement in LULC maps when applying majority voting with random under sampled SVM classifications.

The accuracy of the majority voting was assessed using 1000 random points. The pixel values of the random points were extracted from the majority vote image and each of the individual classifier results. The overall accuracy of each majority image was calculated by dividing the number of majority pixels to the total number of pixels. The accuracy in terms of one majority vote is presented in Table 3.

Table 3. Majority vote overall accuracy.

Year	Ouagadougou	Bobo-Dioulasso
2003	0.88	0.84
2009	0.89	0.86
2015	0.82	0.88
2021	0.86	0.93

The final classification results had some "salt and pepper" effects present due to misclassified pixels. Consequently, a post-classification horizontal majority filter (with a 3×3 neighborhoods) was applied to replace the isolated pixels with the most common neighboring pixel values.

2.8. Land Use/Land Cover Accuracy Assessment

The accuracy of each classified map was assessed directly in GEE, using the error matrix, which is a two-entry table that compares the classified map to the predictions data (Table 4).

Table 4. Error matrix design (Adapted from [49]).

		Prediction						
		1	2	…	j	…	q	Total t_{i+}
Classified map	1	t_{11}	t_{12}	…	t_{1j}	…	t_{1q}	t_{1+}
	2	t_{21}	t_{22}	…	t_{2j}	…	t_{2q}	t_{2+}
	⋮	⋮	⋮	⋮		⋮	⋮	⋮
	i	t_{i1}	t_{i2}		t_{ij}		t_{iq}	t_{i+}
	⋮	⋮	⋮	⋮		⋮	⋮	⋮
	q	t_{q1}	t_{q2}			…	t_{qq}	t_{q+}
	Total t_{+j}	t_{+1}	t_{+2}	…	t_{+j}	…	t_{+q}	

The LULC maps accuracy metrics including overall accuracy (OA) and kappa coefficient (k) were computed based on the error matrix. The overall accuracy is the proportion of all pixel correctly classified in their categories [49]. It is computed according to Equation (1).

$$OA = \frac{\sum_{i=1}^{q} t_{ii}}{N} \times 100 \quad (1)$$

The kappa coefficient which is known to be more robust than the overall accuracy because it takes into account the agreement occurring by chance [50] was also calculated. A value of k below 0 indicates no agreement between the classified map and the observations; 0–20% means a slight agreement; 21–40% corresponds to a fair agreement; 41–60% is a

moderate agreement; 61–80% shows a substantial agreement, and 81–100% indicates an almost perfect agreement [50]. The kappa coefficient is computed following Equation (2).

$$k = \frac{N\sum_{i=1}^{q} t_{ii} - \sum_{i=1}^{q} (t_{i+}t_{+j})}{N^2 - \sum_{i=1}^{q} (t_{i+}t_{+j})} \quad (2)$$

where q is the number of LULC classes, t_{ii} is the number of pixels of class i correctly classified in class i. t_{i+} is the total number of classified pixels in class i, and t_{+j} is the total number of prediction pixels in class j. N is the total number of prediction pixels.

2.9. Land Use/Land Cover Intensity Analysis

Intensity analysis is a mathematical framework that compares a uniform intensity to observed intensities of temporal changes among categories [51]. Uniform intensity is defined as the hypothetical change intensity when the overall change occurred during a time interval was uniformly distributed, from the beginning to the end of the interval [52]. In this study, the categories refer to the different LULC classes, namely built-up, agricultural land, forest, bare land and water. Based on the study years, the time intervals include 2003–2009, 2009–2015 and 2015–2021. Intensity analysis takes place at three levels including interval level, category level and transition level [30]. To perform intensity analysis, in this study, the equations based on Aldwaik and Pontius [52] were used.

The following mathematical notations were used: Y_t corresponds to the year at time point t; Y_{t+1} is the year at time point $t + 1$. J is the number of categories; j is the index for a category at the latter time point of an interval; i is the index for a category at the initial time point of an interval; n is the index of the gaining category for the selected transition; C_{tij} is the size of transition from category i to category j during interval Y_t–Y_{t+1}; C_{tin} is the size of annual transition from i to n during interval Y_t–Y_{t+1}; C_{tnj} is the size of transition from n to j during interval Y_t–Y_{t+1}. C_{tnn} is the size of annual gain of n during interval Y_t–Y_{t+1}.

The interval level analyzes the overall change size and the annual change intensity of the whole area in each time interval. The annual change intensity of the study area during time interval t (S_t) is computed through Equation (3). Equation (4) shows how to compute uniform change intensity during time interval t (U_t). If $S_t < U_t$ then the change is slow. In the case $S_t > U_t$, then the change is fast.

$$S_t = \frac{change\ during\ interval\ t}{study\ area\ size \times interval\ t\ duration} \times 100 = \frac{\sum_{j=1}^{J}\left[\left(\sum_{i=1}^{J} C_{tij}\right) - C_{tij}\right]}{(Y_{t+1} - Y_t)\left(\sum_{j=1}^{J}\sum_{i=1}^{J} C_{tij}\right)} \times 100 \quad (3)$$

$$U_t = \frac{change\ during\ all\ intervals}{study\ area\ size \times study\ duration} \times 100 = \frac{\sum_{t=1}^{T-1}\left(\sum_{j=1}^{J}\sum_{j=1}^{J} C_{tij}\right)}{(Y_T - Y_1)\left(\sum_{j=1}^{J}\sum_{i=1}^{J} C_{tij}\right)} \times 100 \quad (4)$$

The category level deals with the variation in size and intensity of gross gains and gross losses across categories during each time period. The loss intensity (L_{ti}) from a category i is the lost percentage of the start size of that category i during the time interval t (Equation (5)). The gain intensity (G_{tj}) to a category j corresponds to the percentage of the end size of that category j that gained during the time interval t (Equation (6)). The intensity of a uniform change during time interval t is defined by S_t (Equation (3)). If $L_{ti} < S_t$ or $G_{tj} < S_t$, then the loss from category i or gain to category j during time interval t is dormant. If $L_{ti} > S_t$ or $G_{tj} > S_t$, then the loss from category i or gain to category j during time interval t is active.

$$L_{ti} = \frac{loss\ of\ category\ i\ during\ interval\ t}{interval\ t\ duration \times size\ of\ category\ i\ at\ start\ of\ intervalt} \times 100 = \frac{\sum_{i=1}^{J} C_{tij} - C_{tii}}{(Y_{t+1} - Y_t)\sum_{i=1}^{J} C_{tij}} \times 100 \quad (5)$$

$$G_{tj} = \frac{gain\ of\ category\ j\ during\ interval\ t}{interval\ t\ duration \times size\ of\ category\ j\ at\ end\ of\ interval\ t} \times\ 100 = \frac{\sum_{i=1}^{J} C_{tij} - C_{tjj}}{(Y_{t+1} - Y_t)\sum_{j=1}^{J} C_{tij}} \times 100 \quad (6)$$

The transition level computes for each category how the size and intensity of a given category's transitions vary across the other categories which are available for the transition [51]. The transition intensity from category i to category n during time-interval t (R_{tin}), where i is different from n, is defined by Equation (7). Equation (8) presents the uniform or hypothetical transition intensity to category n during time interval t (W_{tn}). In the case $R_{tin} < W_{tn}$, then the gain or loss of n avoids i during interval t. If $R_{tin} > W_{tn}$, then the gain or loss of n targets i during time interval t.

$$R_{tin} = \frac{transition\ area\ from\ category\ i\ to\ n\ during\ interval\ t}{interval\ t\ duration \times size\ of\ category\ i\ at\ start\ time} \times 100 = \frac{C_{tin}}{(Y_{t+1} - Y_t)\sum_{j=1}^{J} C_{tij}} \times 100 \quad (7)$$

$$W_{tn} = \frac{gain\ of\ category\ n\ during\ interval\ t \times 100}{interval\ t\ duration \times size\ of\ non\ category\ n\ at\ start\ time} = \frac{\sum_{i=1}^{J} C_{tin} - C_{tnn} \times 100}{(Y_{t+1} - Y_t)\sum_{j=1}^{J}\left[\left(\sum_{i=1}^{J} C_{tij}\right) - C_{tnj}\right]} \quad (8)$$

To perform the intensity analysis, the "OpenLand"package [53] in *R* environment was used. The LULC results from the four years were used as input data in the "contingencyTable" to generate a cross-tabulated matrix comprising the quantity of changes in square kilometers from one category to another between two consecutive time points. This cross-tabulated matrix was utilized as input in the "intensityAnalysis" function to compute the interval, category and transition levels of changes that occurred between the different categories, during the three-time intervals. Figure 2 presents the overall methodological flowchart of the study.

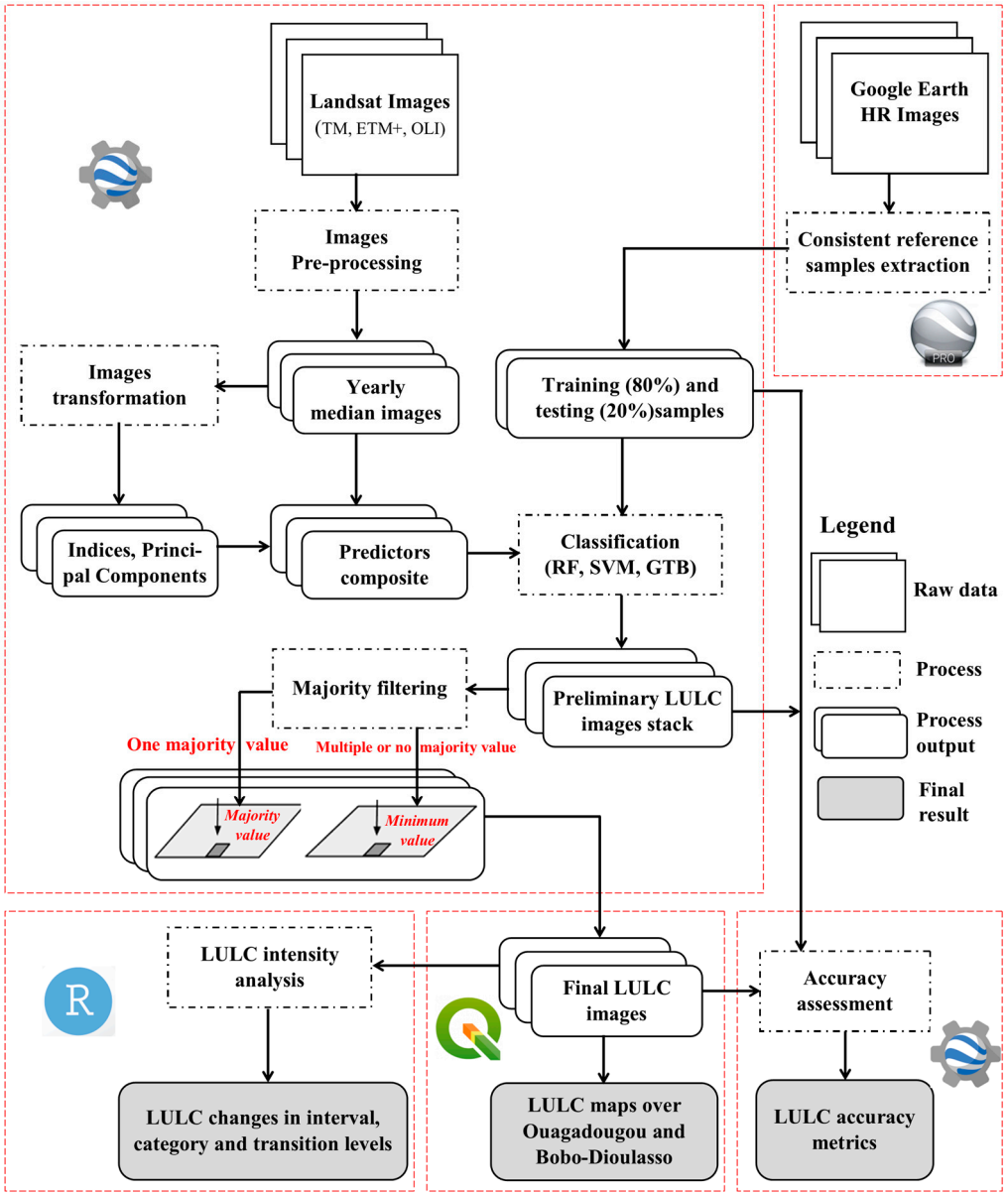

Figure 2. Methodological flowchart of the LULC mapping.

3. Results

3.1. LULC Classification Accuracy

The classified LULC images accuracies were assessed using the overall accuracy and the kappa coefficient. The individual classifications overall accuracy varied between 0.8 (RF 2021) and 0.94 (RF 2003) in Ouagadougou, while in Bobo-Dioulasso, it was between 0.66 (RF 2015) and 0.77 (SVM 2003). The majority voting results showed smoothed overall accuracies and kappa coefficients for all the years in Ouagadougou (Table 5). However, there is an improvement for both metrics, compared to the results of all the individual classifiers in 2009. For Bobo-Dioulasso, the majority voting images presented stable (2009 and 2015) to totally improved values (2003 and 2021) compared to the individual classifiers for the overall accuracy and the kappa coefficient (Table 6).

Table 5. LULC Accuracy metrics in Ouagadougou.

Year	RF	GTB	SVM	Majority	RF	GTB	SVM	Majority
	Overall Accuracy				kappa coefficient			
2003	0.94	0.89	0.82	0.87	0.9	0.81	0.69	0.79
2009	0.81	0.8	0.85	0.87	0.68	0.66	0.74	0.79
2015	0.85	0.87	0.85	0.85	0.74	0.77	0.75	0.77
2021	0.8	0.83	0.92	0.82	0.66	0.72	0.87	0.72

Table 6. LULC Accuracy metrics in Bobo-Dioulasso.

Year	RF	GTB	SVM	Majority	RF	GTB	SVM	Majority
	Overall Accuracy				kappa coefficient			
2003	0.66	0.71	0.77	0.81	0.52	0.6	0.7	0.75
2009	0.74	0.71	0.74	0.74	0.63	0.58	0.64	0.64
2015	0.66	0.74	0.74	0.74	0.52	0.64	0.63	0.64
2021	0.71	0.78	0.71	0.85	0.57	0.69	0.59	0.79

3.2. Land Use/Land Cover Spatial Distribution

The LULC maps in Ouagadougou (Figure 3) show that the dominant classes are agricultural land and built-up area. There was a continuous expansion of settlement areas from the inner city towards the peripheral areas at the expense of other land uses such as agricultural areas. Being the two main land use classes in the area, they have a negative correlation in terms of spatial growth. While built-up land is expanding in the area, agricultural land area is decreasing, indicating the intensification of human footprint throughout the years. Other Land Use/Land Cover classes such as water bodies, forest and bare land were also present in the maps. In Bobo-Dioulasso, agricultural land, forest and built areas are the most represented (Figure 4). Like Ouagadougou, settlement areas in Bobo-Dioulasso kept growing, to the detriment of natural landscape such as forest areas. The expansion of built-up areas towards the northern side of the city of Bobo-Dioulasso is due to the development of a new estate, named "Bobo 2010", by the year 2007 at that part. The water bodies and bare land areas occupy small surfaces in the maps.

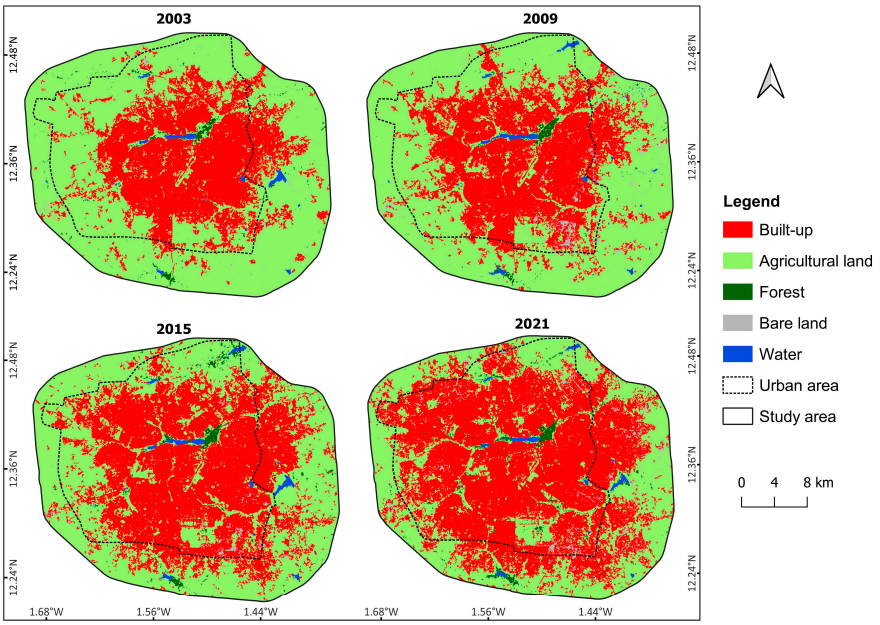

Figure 3. Land Use/Land Cover distribution in Ouagadougou.

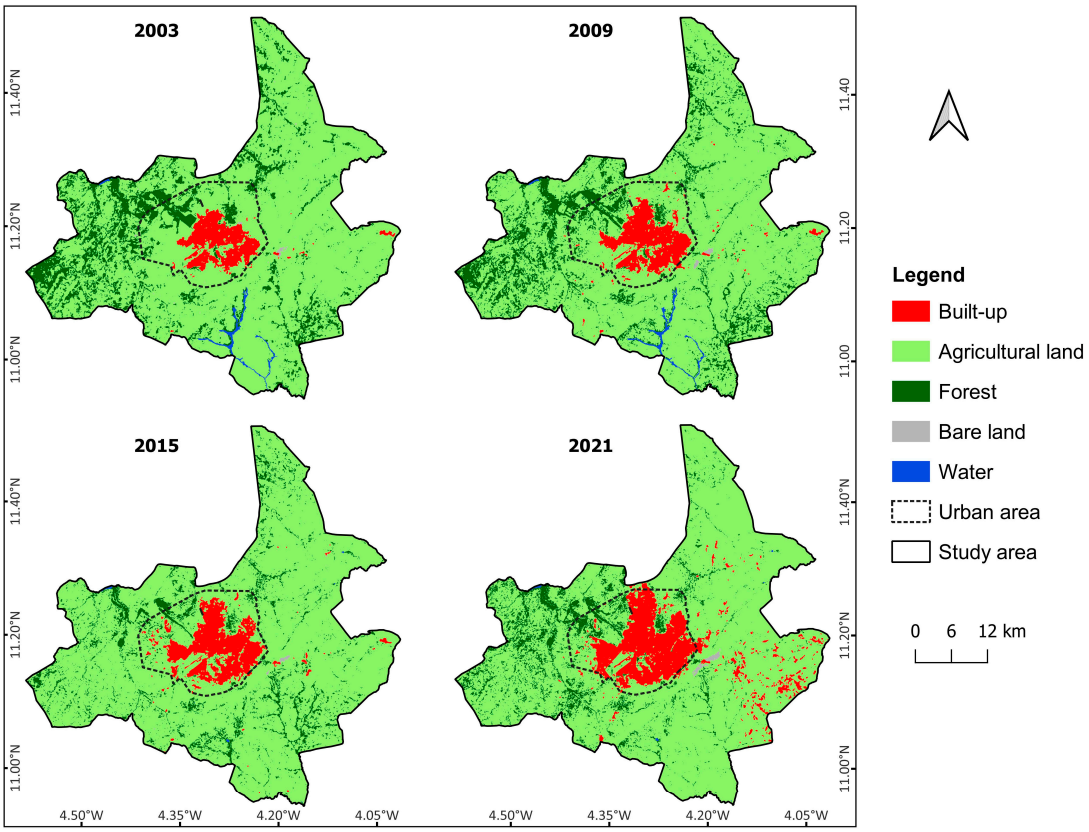

Figure 4. Land Use/Land Cover distribution in Bobo-Dioulasso.

3.3. LULC Trend

The landscape units have changed in different ways between 2003 and 2021 in Ouagadougou and Bobo-Dioulasso (Figure 5). In Ouagadougou, the built-up area occupied 32.75%, 35.95%, 46.86% and 58.34% of the total landscape in 2003, 2009, 2015 and 2021, respectively. Conversely, the agricultural land areas had a decreasing trend represented by 65.45%, 60.86%, 50.13% and 37.80% of the area in 2003, 2009, 2015 and 2021, respectively. These figures indicate a linear increase of 78.13% for built-up area against a decrease of 42.25% for agricultural land between 2003 and 2021. The forest areas experienced an increase of 55.56%, while the water bodies increased by 2.84% due to the construction of a new dame in the northern part of the study area in 2007. Bare land surfaces also increased consequently and occupied more than 19% of the landscape in 2021.

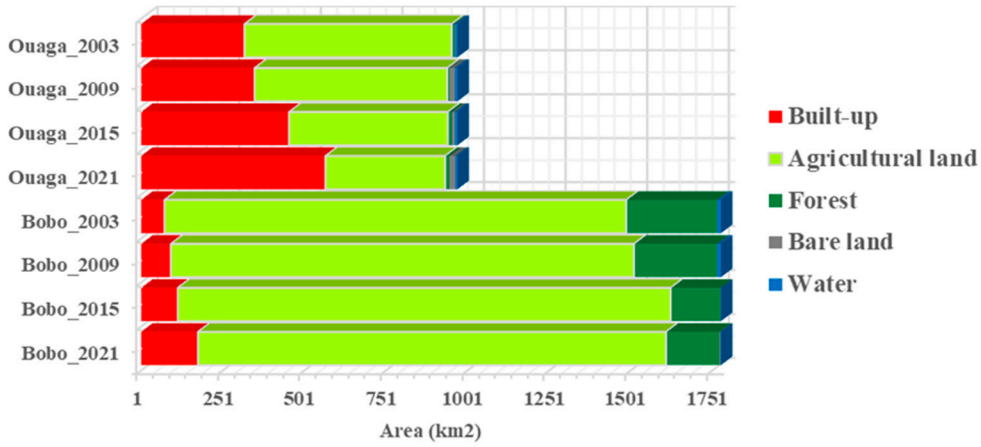

Figure 5. Land Use/Land Cover evolution between 2003 and 2021.

In Bobo-Dioulasso, like Ouagadougou, the built-up areas continuously increased during the study time span. The built-up areas represented 4.10%, 5.19%, 6.36% and 9.86% of the total area in 2003, 2009, 2015 and 2021, respectively, corresponding to a variation of +140.7% during the study period. Unlike Ouagadougou, the trend of agricultural lands was not steady in Bobo-Dioulasso. There was a gradual growth from 79.59% (2003) to 79.85% (2009) and 84.99% (2015) and a decline to 80.69% (2021). The decrease of agricultural land in 2021 could be due to the 0.68% increase of forest area after a continuous decline from 15.58% (2003) to 8.51% (2015). The bare land had a global increase, whereas the water bodies decreased across the study period.

3.4. LULC intensity Analysis

3.4.1. Interval Level

Figure 6 shows the graphical representation of the interval level analysis results, which compare annual changes intensity of all the area within each time interval. A fast annual change intensity was recorded in Ouagadougou between 2015 and 2021 (3.61% per year against 3.09% as uniform intensity), while in Bobo-Dioulasso it was fast between 2009 and 2015 (2.22%, compared to a uniform intensity of 2.17%). During the two other time periods, 2003–2009 and 2009–2015 for Ouagadougou and 2003–2009 and 2015–2021 for Bobo-Dioulasso, the annual intensity of change was slow.

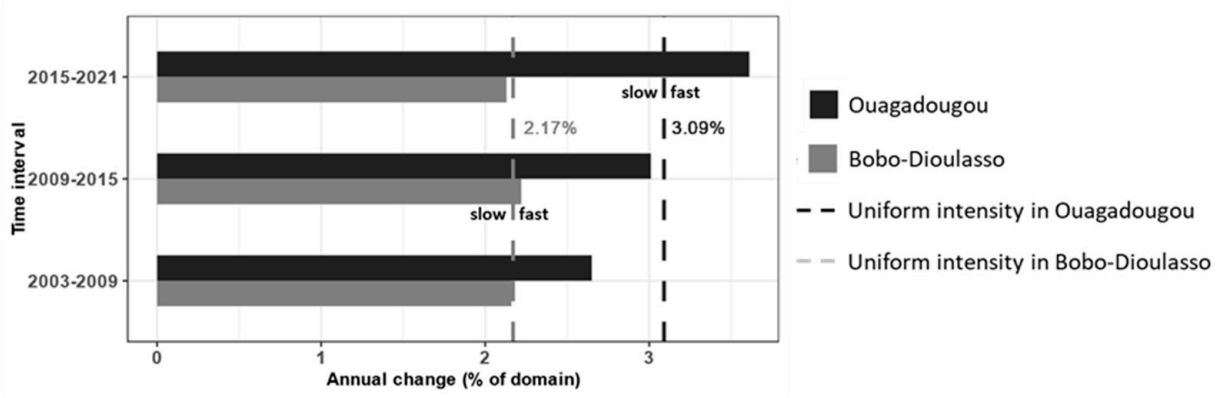

Figure 6. Interval level changes of Land Use/Land Cover categories (The annual change rate is expressed in percentage of the total area).

3.4.2. Category Level

The category level analysis plots present the size and annual intensity of change of each category's gain relative to the size of the category at the interval's end time point. It also shows the size and annual intensity of each category's loss in relation to the size of the category at the interval's initial time point. Figure 7a,b presents the graphical outputs of category analysis for each time interval in Ouagadougou. The built-up class was the largest gainer during all the time intervals, followed by bare and agricultural lands. Built-up gain increased continuously, from 8.6% in 2003–2009 and 13.68% in 2009–2015 to achieving 15.73% of the total landscape in 2015–2021. As for the annual change intensity, the uniform intensity (S_t) values indicated an intensification of change from 2003–2009 (2.65%) to 2015–2021 (3.61%). Bare, forest and built-up classes had active changes during the three-time intervals, with bare having the most active gain ($G_{tj} > S_t$) in 2003–2009 and 2015–2021, while forest gain was very active in 2009–2015 and 2015–2021. The water class showed active gain in 2003–2009 and 2009–2015. Concerning agricultural category, the gain intensity was dormant ($G_{tj} < S_t$) throughout the time. In terms of loss in Ouagadougou, agricultural land had the largest loss in terms of area during the three-time intervals, followed by built-up and bare. Agricultural loss increased, going from 9.64% in 2003–2009 and 13.63% in 2009–2015 to 15.91% in 2015–2021. The active loss rates were recorded by agricultural, forest, bare and water classes during 2009–2015 and 2015–2021. The built-up class was

dormant, except in 2003–2009, where it showed a marginal loss in favor of bare land. Looking at the behavior of each bar regarding the uniform rate, it emerged that less than half of the bar length for agricultural lands in 2009–2015 and 2015–2021 extend beyond the uniform rate, showing that the large size of area occupied by agricultural in 2009 and 2015 is the cause of its large loss. In 2003–2009, more than 50% of forest and water bar lengths exceeds the uniform rate, indicating that active change intensity is the reason explaining the two categories' losses sizes. In each time interval, more than half of the bare land goes beyond the uniform line, demonstrating that active intensity is more important than the size of bare land at the start time to explain the size of bare land's loss.

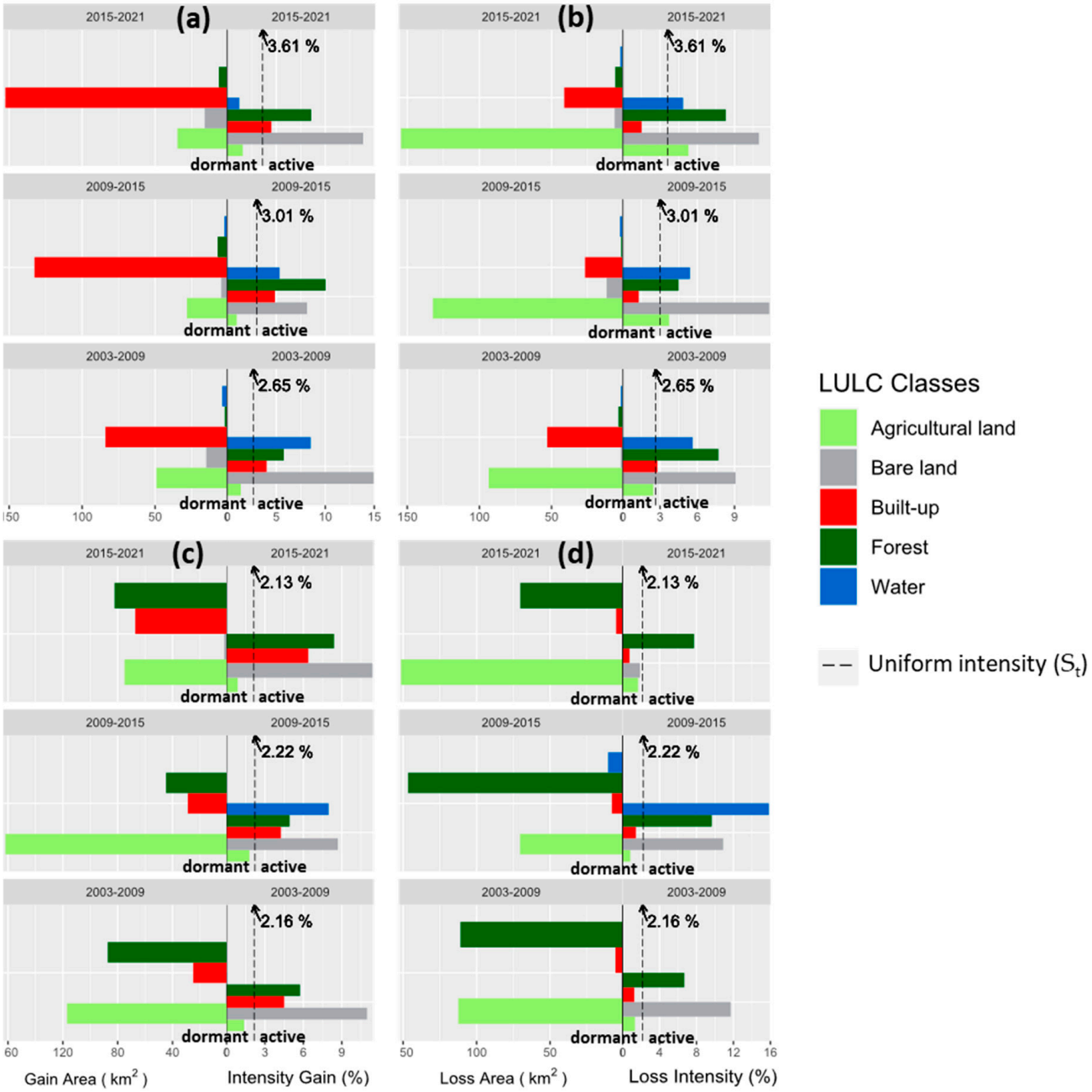

Figure 7. Category level changes of land use/cover and: (**a**) gain in Ouagadougou, (**b**) loss in Ouagadougou, (**c**) gain in Bobo-Dioulasso, (**d**) loss in Bobo-Dioulasso.

Figure 7c,d shows the category level analysis plot in terms of size and intensity of change for Bobo-Dioulasso. The larger gainers, in size, were, respectively, agricultural, forest and built-up classes during the three periods. The gains in agricultural land increased from 2003 (6.58%) to 2015 (9.11%) and decreased in 2021 (4.22%) at the expense of forest area, which nearly doubled its gain compared to 2015 (2.52% to 4.63%). Built-up surface gains increased regularly during the different time intervals, going from 1.4% in 2003–2009 to 3.78% in 2015–2021. The uniform rate showed a quasi-stationary intensity of change during the different time intervals. As for the gain intensity, bare land, forest and built-up areas experienced the most active changes ($G_{tj} > S_t$). Agricultural change was dormant throughout the time. In terms of loss, agricultural and forest areas were the larger losers. The intensity of loss for the forest category was active during the three periods. Bare land also experienced active loss during 2009–2015 and 2015–2021. The large loss in forest and bare areas could be explained by the very active change intensity because more than 50% of the bar lengths exceeds the uniform intensity rate. Agricultural land and built-up surfaces showed a dormant change during the period.

3.4.3. Transition Level

Figure 8 shows the transition level changes for built-up gain and agricultural loss in Ouagadougou and Bobo-Dioulasso. The transition level analyses focused on built-up and agricultural categories because they are the dominant classes in the study area throughout the four time points. The gain and loss intensities are analyzed regarding the deviation of each category intensity from the uniform intensity. When a category intensity is higher than the uniform intensity, the transition targets that category, and when a category intensity is less than the uniform intensity, the transition avoids that category.

In Ouagadougou, the gain of built-up area targeted bare and agricultural lands ($R_{tin} > W_{tn}$) in all the time intervals (Figure 8a). The other classes were avoided ($R_{tin} < W_{tn}$). The major transition to built-up category came from bare land, with an increasing intensity (R_{tin}) going from 6.81% in 2003–2009 to 9.91% in 2009–2015 and 10.04% in 2015–2021. That could be explained by the greater transition intensity of bare land which largely exceeds the uniform line. As for agricultural loss, it targeted forest in all the time interval, while in 2003–2009, and 2009–2015, water was also converted to agricultural (Figure 8b). In addition, bare land in 2003–2009 and slightly built-up in 2015–2021 were gaining from agricultural. The major gainer from agriculture was forest, with a peak intensity in 2009–2015.

In Bobo-Dioulasso, the built-up class only gained from bare and agricultural lands (Figure 8c). Indeed, the bare land class was targeted in 2003–2009 and 2009–2015 (R_{tin} =4.61% and 1.34%, respectively), while in 2015–2021 the agricultural class took over and started getting targeted (R_{tin} = 0.74%) by the built-up class. The explanation of such a situation could be that people used all the bare land areas for building and started exploiting agricultural lands. It could also be caused by classification errors resulting in a confusion between bare and agricultural lands.

The loss of agricultural land area occurred in favor of forest, bare land and built-up lands (Figure 8d). The loss targeted ($R_{tin} > W_{tn}$) bare land and forest. Built-up gain from the agricultural class was avoided in Bobo-Dioulasso. This could be explained by the fact that the over-exploited agricultural areas became degraded and appeared as bare land. A few of these areas are used for building, pavement and road construction.

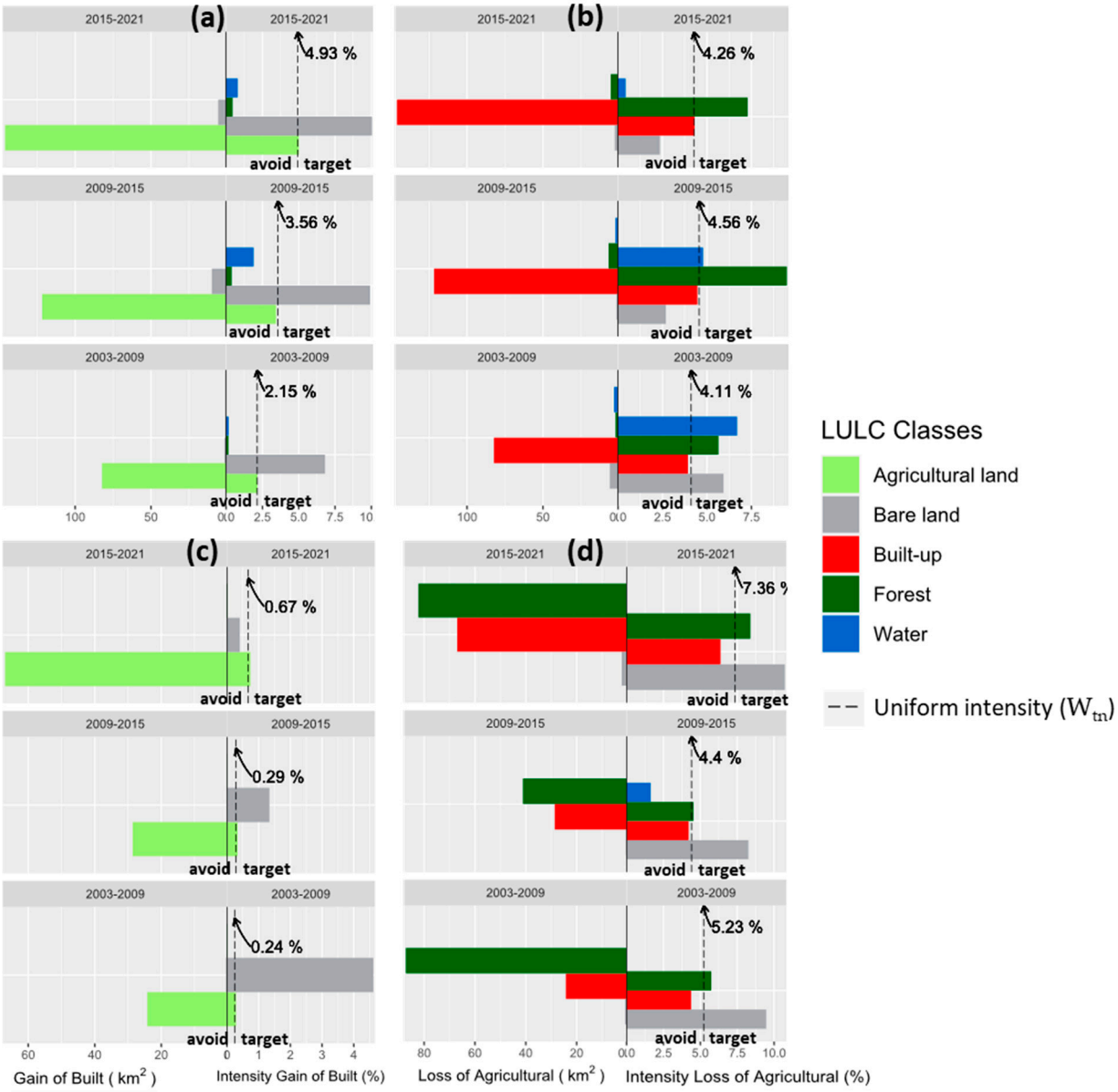

Figure 8. Transition level changes of Land Use/Land Cover: (**a**) gain of built-up in Ouagadougou, (**b**) loss of agricultural in Ouagadougou, (**c**) gain of built-up in Bobo-Dioulasso, (**d**) loss of agricultural in Bobo-Dioulasso.

4. Discussion

4.1. LULC Changes in the Study Area

The analysis of LULC patterns showed that the landscape experienced changes towards built-up area increase at the expense of agricultural lands (cultivated lands including seasonal, permanent crops and fallows, shrubland and grassland) and bare land in Ouagadougou and in Bobo-Dioulasso. These dynamics indicate the ongoing urbanization induced human footprint intensification in the areas. The urbanization process in the area is characterized by the horizontal expansion of the cities and an increasing population due to natural growth, rural–urban migration and smaller town to larger city migration. For example, in 2019, Ouagadougou and Bobo-Dioulasso concentrated 45.1% and 16.9% of the country's total urban population, respectively [17], with a net migration rate of 4% per year in Ouagadougou [19]. This rapid urban population growth could be one the driving factor of the landscape changes, as rapid population increase causes high demand in land and consequently leads to LULC changes [54]. The changes of LULC classes in favor of built-up

areas were also recorded in other urban settings [9,16,55]. Furthermore, the conversion of agricultural land to roads (a component in built-up class) causes the displacement of arborists with their trees to resettle along the road-faced walls of some administrations.

4.2. Built-Up Expansion in the Study Area

The city of Ouagadougou is experiencing a rapid settlement expansion, while in Bobo-Dioulasso, the built-up area increasing is slow. The cities have extended beyond their administrative boundaries into surrounding districts or villages, particularly in Ouagadougou. A similar situation was reported for Kumasi metropolitan city (Ghana), where urban development was found to have gone beyond its official boundaries [6]. Due to the adverse impacts of climate change, causing difficulties in finding alternative non-agricultural livelihood options, the rural population migrates to the cities to look for new sources of livelihood. Once in the city, not having resources to afford good housing, they settle in the peripheral slum's areas, making the city expand horizontally. Since the new population is coming into the city, the number of inhabitants increased year by year. It is reported that Ouagadougou welcomes around 100,000 additional people per year [56], and given the insufficient housing offer policy, most of the newcomers establish their houses in the peri-urban areas. This situation contributes to the development of informal neighborhoods around the city. Furthermore, since 2009 there has been a land speculation process driven by private real estate companies. Indeed, with the authorizations from the government agencies, they buy land at low-cost prices from farmers in the peripheral areas, subdivide it into plots and sell to individuals. From 2009 to 2019, a total of 275 land/real estate development approvals were issued to private companies [19]. This context of high demand of land for construction linked to population growth leads to an increasing expansion of built-up areas [57].

The rapid expansion of built-up areas has potential negative implications on urban agricultural production. This is because areas previously used for urban gardening, the water pathways and the urban green areas are being converted to concrete buildings. That conversion process also leads to an increase in impervious surfaces exposing the population to hazards such as flooding and the Urban Heat Island effect [58]. In addition, the rapid urban settlement expansion has resulted in limited goods and services provision in the peripheral areas [59], highlighting the inadequacy between the urban development and economic growth in most cities in the developing world [8]. The World Bank revealed that in unplanned areas around cities, the quality of life is deteriorated due to the poor housing systems, insufficient road network and inadequate water and sanitation supply [60]. This situation was also reported by the United Nations which stated that rapid urban growth and its inherent consequences are a common phenomenon for many African cities because they are expected to record the highest growth rate in the coming 30 years [2].

The LULC dynamics may have some uncertainties due to the low number of samples and the aggregation of some classes into one (as in the case of seasonal croplands, permanent croplands, fallowlands, shrublands and grasslands which were combined to form the agricultural land class). In this study, more samples were collected in Ouagadougou than Bobo-Dioulasso due to the limited availability of clear high-resolution historical images in Google Earth. This situation may have affected the accuracy of the classification results, particularly in Bobo-Dioulasso, which showed low overall accuracies across the four years. In addition, the majority filtering bias is towards the classes labeled with least values (minimum values were returned in cases where there are no majority votes). However, the bias level is relatively low given the high accuracy values of the majority images (>80% in both sites) and the fact that the area is dominated by built-up (in Ouagadougou) and agricultural lands (in Bobo-Dioulasso). The use of more samples could improve the classifications accuracies and allow the capturing of more detailed LULC classes in the area.

5. Conclusions

The advent of geospatial cloud-computing platforms such as Google Earth Engine is revolutionizing the use of remote sensing for LULC studies. This study combined remote sensing and GIS techniques with intensity analysis approach to assess the LULC dynamics in Bobo-Dioulasso and Ouagadougou. The changes were analyzed by means of intensity analysis at three level including interval, category and transition in three-time intervals namely 2003–2009, 2009–2015 and 2015–2021. The results showed that Ouagadougou experienced a fast annual change intensity during the period 2015–2021, whereas in Bobo-Dioulasso, a fast intensity was recorded during the period 2009–2015. The transition of changes was towards built-up surfaces at the expense of bare and agricultural lands in the two cities. Concretely, the patterns of LULC transitions caused an increasing trend of built-up units in both cities, while agricultural land decreased in Ouagadougou and slightly increased in Bobo-Dioulasso. The built-up area grew by 78.13% and 140.67%, respectively, in Ouagadougou and Bobo-Dioulasso, while agricultural land lost 42.24% of its area in Ouagadougou and gained 1.38% area in Bobo-Dioulasso. The increase in built-up areas at the expense of agricultural indicates a modification of the surface properties, which could alter the living conditions of urban dwellers. The settlement sprawling towards the peripheral areas poses the problem of goods and services provision to the population, which is a common threat to cities in developing countries. The outcomes of this study present the pattern, size and intensity of urbanization-induced LULC changes and could be used as guide for sustainable urban land use planning. However, further investigations could be carried out in the area using more training samples to reduce the level of uncertainties and map LULC in detail for urbanization modeling in the region.

Author Contributions: This research has been designed by V.O., K.O.H., M.T., J.D. and V.O. processed the data with help and suggestions from K.O.H. and M.T. The manuscript was written by V.O. with inputs from all co-authors. All authors have read and agreed to the published version of the manuscript.

Funding: This work forms part of a Ph.D. research which is funded by the German Federal Ministry of Education and Research (BMBF) through the West African Science Service Centre on Climate Change and Adapted Land Use (WASCAL).

Institutional Review Board Statement: Not Applicable.

Informed Consent Statement: Not applicable.

Data Availability Statement: Data in WASCAL are open access and are made available upon the receipt of an official request to the institution through the Data Management Department.

Acknowledgments: The authors are grateful to the German Federal Ministry of Education and Research for funding this research. We acknowledge the West African Science Service Centre on Climate Change and Adapted Land Use for the management of the program. We also appreciate the Federal University of Technology, Minna, Niger State, Nigeria, host institution of the Doctoral Research Programme (DRP) on Climate Change and Human Habitat.

Conflicts of Interest: The authors have not declared any conflict of interest.

References

1. Kuddus, M.A.; Tynan, E.; McBryde, E. Urbanization: A problem for the rich and the poor? *Public Health Rev.* **2020**, *41*, 1. [CrossRef]
2. United Nations. World Urbanization Prospects; 2018; Volume 12. Available online: https://population.un.org/wup/Publications/Files/WUP2018-Report.pdf (accessed on 9 May 2022).
3. Huang, K.; Li, X.; Liu, X.; Seto, K.C. Projecting global urban land expansion and heat island intensification through 2050. *Environ. Res. Lett.* **2019**, *14*, 114037. [CrossRef]
4. Schug, F.; Okujeni, A.; Hauer, J.; Hostert, P.; Nielsen, J.; van der Linden, S. Mapping patterns of urban development in Ouagadougou, Burkina Faso, using machine learning regression modeling with bi-seasonal Landsat time series. *Remote Sens. Environ.* **2018**, *210*, 217–228. [CrossRef]
5. Güneralp, B.; Lwasa, S.; Masundire, H.; Parnell, S.; Seto, K.C. Urbanization in Africa: Challenges and opportunities for conservation. *Environ. Res. Lett.* **2017**, *13*, 015002. [CrossRef]

6. Hackman, K.O.; Li, X.; Asenso-Gyambibi, D.; Asamoah, E.A.; Nelson, I.D. Analysis of geo-spatiotemporal data using machine learning algorithms and reliability enhancement for urbanization decision support. *Int. J. Digit. Earth* **2020**, *13*, 1717–1732. [CrossRef]
7. Stemn, E.; Kumi-Boateng, B. Modelling of land surface temperature changes as determinant of urban heat island and risk of heat-related conditions in the Wassa West Mining Area of Ghana. *Model. Earth Syst. Environ.* **2020**, *6*, 1727–1740. [CrossRef]
8. Cohen, B. Urbanization in developing countries: Current trends, future projections, and key challenges for sustainability. *Technol. Soc.* **2006**, *28*, 63–80. [CrossRef]
9. Rimal, B.; Zhang, L.; Keshtkar, H.; Haack, B.N.; Rijal, S.; Zhang, P. Land use/land cover dynamics and modeling of urban land expansion by the integration of cellular automata and markov chain. *ISPRS Int. J. Geo-Inf.* **2018**, *7*, 154. [CrossRef]
10. Fonseka, H.P.U.; Zhang, H.; Sun, Y.; Su, H.; Lin, H.; Lin, Y. Urbanization and its impacts on land surface temperature in Colombo Metropolitan Area, Sri Lanka, from 1988 to 2016. *Remote Sens.* **2019**, *11*, 957. [CrossRef]
11. Kafy, A.A.; Rahman, M.S.; Faisal, A.A.; Hasan, M.M.; Islam, M. Modelling future land use land cover changes and their impacts on land surface temperatures in Rajshahi, Bangladesh. *Remote Sens. Appl. Soc. Environ.* **2020**, *18*, 100314. [CrossRef]
12. Sannigrahi, S.; Bhatt, S.; Rahmat, S.; Uniyal, B.; Banerjee, S.; Chakraborti, S.; Jha, S.; Lahiri, S.; Santra, K.; Bhatt, A. Analyzing the role of biophysical compositions in minimizing urban land surface temperature and urban heating. *Urban Clim.* **2017**, *24*, 803–819. [CrossRef]
13. McCarthy, M.P.; Best, M.J.; Betts, R.A. Climate change in cities due to global warming and urban effects. *Geophys. Res. Lett.* **2010**, *37*, 1–5. [CrossRef]
14. Faichia, C.; Tong, Z.; Zhang, J.; Liu, X. Using RS Data-Based CA—Markov Model for Dynamic Simulation of Historical and Future LUCC in Vientiane, Laos. *Sustainability* **2020**, *12*, 8410. [CrossRef]
15. Hamad, R.; Balzter, H.; Kolo, K. Predicting land use/land cover changes using a CA-Markov model under two different scenarios. *Sustainability* **2018**, *10*, 3421. [CrossRef]
16. Mahmoud, M.I.; Duker, A.; Conrad, C.; Thiel, M.; Ahmad, H.S. Analysis of settlement expansion and urban growth modelling using geoinformation for assessing potential impacts of urbanization on climate in Abuja City, Nigeria. *Remote Sens.* **2016**, *8*, 220. [CrossRef]
17. INSD. *Cinquième Recensement Général de La Population et de l'Habitation Du Burkina Faso*; INSD: Ouagadougou, Burkina Faso, 2022.
18. Sory, I. « Ouaga la Belle ! » Gestion des Déchets Solides à Ouagadougou: Enjeux Politiques, Jeux D'acteurs et Inégalités Environnementales. Ph.D. Thesis, Université Paris I Panthéon Sorbonne, Paris, France, 2013.
19. Sory, I. Public land policies at an impasse in Ouagadougou (Burkina Faso). *Afr. Contemp.* **2019**, *269*, 135–154.
20. Hauer, J.; Østergaard Nielsen, J.; Niewöhner, J. Landscapes of hoping—Urban expansion and emerging futures in Ouagadougou, Burkina Faso. *Anthropol. Theory* **2018**, *18*, 59–80. [CrossRef]
21. Oñate-valdivieso, F.; Oñate-paladines, A.; Collaguazo, M. Spatiotemporal Dynamics of Soil Impermeability and Its Impact on the Hydrology of An Urban Basin. *Land* **2022**, *11*, 250. [CrossRef]
22. Rimal, B.; Zhang, L.; Keshtkar, H.; Wang, N.; Lin, Y. Monitoring and modeling of spatiotemporal urban expansion and land-use/land-cover change using integrated Markov chain cellular automata model. *ISPRS Int. J. Geo-Inf.* **2017**, *6*, 288. [CrossRef]
23. Sarfo, I.; Shuoben, B.; Darko, G.; Adu, E.; Kedjanyi, G.; Oduro, C.; Folorunso, E.A.; Alriah, M.A.A.; Amankwah, S.O.Y.; Ndafira, G.C. Validating local drivers influencing land use cover change in Southwestern Ghana: A mixed-method approach. *Environ. Earth Sci.* **2022**, *81*, 367. [CrossRef]
24. Temgoua, L.F.; Allaissem, B.; Tchamba, M.; Saradoum, G.; Osée, M.M.; Caroline, M. Spatio-Temporal Dynamic of Land Use and Land Cover in the Classified Forest of Djoli-Kera, South-Eastern, Chad. *Open J. For.* **2018**, *8*, 283–296. [CrossRef]
25. Amani, M.; Ghorbanian, A.; Ahmadi, S.A.; Kakooei, M.; Moghimi, A.; Mirmazloumi, S.M.; Moghaddam, S.H.A.; Mahdavi, S.; Ghahremanloo, M.; Parsian, S.; et al. Google Earth Engine Cloud Computing Platform for Remote Sensing Big Data Applications: A Comprehensive Review. *IEEE J. Sel. Top. Appl. Earth Obs. Remote Sens.* **2020**, *13*, 5326–5350. [CrossRef]
26. Gorelick, N.; Hancher, M.; Dixon, M.; Ilyushchenko, S.; Thau, D.; Moore, R. Google Earth Engine: Planetary-scale geospatial analysis for everyone. *Remote Sens. Environ.* **2017**, *202*, 18–27. [CrossRef]
27. Yang, L.; Driscol, J.; Sarigai, S.; Wu, Q.; Chen, H.; Lippitt, C.D. Google Earth Engine and Artificial Intelligence (AI): A Comprehensive Review. *Remote Sens.* **2022**, *14*, 3253. [CrossRef]
28. Nababa, I.I.; Symeonakis, E.; Koukoulas, S.; Higginbottom, T.P.; Cavan, G.; Marsden, S. Land cover dynamics and mangrove degradation in the niger delta region. *Remote Sens.* **2020**, *12*, 3619. [CrossRef]
29. Abu, I.O.; Szantoi, Z.; Brink, A.; Robuchon, M.; Thiel, M. Detecting cocoa plantations in Côte d'Ivoire and Ghana and their implications on protected areas. *Ecol. Indic.* **2021**, *129*, 107863. [CrossRef]
30. Quan, B.; Pontius, R.G.; Song, H. Intensity Analysis to communicate land change during three time intervals in two regions of Quanzhou City, China. *GIScience Remote Sens.* **2019**, *57*, 21–36. [CrossRef]
31. INSD. *Recensement General de La Population et de l'habitation de 2006*; INSD: Ouagadougou, Burkina Faso, 2006.
32. USGS. *Landsat Collection 1 vs. Collection 2 Summary*; USGS: Reston, VA, USA, 2020; Volume 2.
33. Asare, Y.M.; Forkuo, E.K.; Forkuor, G.; Thiel, M. Evaluation of gap-filling methods for Landsat 7 ETM+ SLC-off image for LULC classification in a heterogeneous landscape of West Africa. *Int. J. Remote Sens.* **2020**, *41*, 2544–2564. [CrossRef]
34. Forkuor, G.; Dimobe, K.; Serme, I.; Tondoh, J.E. Landsat-8 vs. Sentinel-2: Examining the added value of sentinel-2's red-edge bands to land-use and land-cover mapping in Burkina Faso. *GIScience Remote Sens.* **2018**, *55*, 331–354. [CrossRef]

35. Rasul, A.; Balzter, H.; Ibrahim, G.R.F.; Hameed, H.M.; Wheeler, J.; Adamu, B.; Ibrahim, S.; Najmaddin, P.M. Applying built-up and bare-soil indices from Landsat 8 to cities in dry climates. *Land* **2018**, *7*, 81. [CrossRef]
36. Polykretis, C.; Grillakis, M.G.; Alexakis, D.D. Exploring the impact of various spectral indices on land cover change detection using change vector analysis: A case study of Crete Island, Greece. *Remote Sens.* **2020**, *12*, 319. [CrossRef]
37. Tassi, A.; Vizzari, M. Object-oriented lulc classification in google earth engine combining snic, glcm, and machine learning algorithms. *Remote Sens.* **2020**, *12*, 3776. [CrossRef]
38. Appiah, D.O. Geoinformation Modelling of Peri-Urban Land Use and Land Cover Dynamics for Climate Variability and Climate Change in the Bosomtwe District, Ghana. Ph.D. Thesis, WASCAL, Ouagadougou, Burkina Faso, 2016.
39. Di Gregorio, A.; Jansen, L.J.M.; Di Gregorio, A.; Jansen, L.J.M. *Land Cover Classification System (LCCS): Classification Concepts and User Manual*; FAO: Rome, Italy, 2000; Volume 53, p. 179.
40. Gholamy, A.; Kreinovich, V.; Kosheleva, O. Why 70/30 or 80/20 Relation between Training and Testing Sets: A Pedagogical Explanation. *Dep. Tech. Rep.* **2018**, *1209*, 1–6.
41. Breiman, L. Random Forests. *Mach. Learn.* **2001**, *45*, 5–32. [CrossRef]
42. Cracknell, M.J.; Reading, A.M. Geological mapping using remote sensing data: A comparison of five machine learning algorithms, their response to variations in the spatial distribution of training data and the use of explicit spatial information. *Comput. Geosci.* **2014**, *63*, 22–33. [CrossRef]
43. Nery, T.; Sadler, R.; Solis-Aulestia, M.; White, B.; Polyakov, M.; Chalak, M. Comparing supervised algorithms in Land Use and Land Cover classification of a Landsat time-series. *Int. Geosci. Remote Sens. Symp.* **2016**, *2016*, 5165–5168. [CrossRef]
44. Forkuor, G.; Conrad, C.; Thiel, M.; Landmann, T.; Barry, B. Evaluating the sequential masking classification approach for improving crop discrimination in the Sudanian Savanna of West Africa. *Comput. Electron. Agric.* **2015**, *118*, 380–389. [CrossRef]
45. Zoungrana, B.J.; Conrad, C.; Amekudzi, L.K.; Thiel, M.; Da, E.D. Land Use/Cover Response to Rainfall Variability: A Comparing Analysis between NDVI and EVI in the Southwest of Burkina Faso. *Climate* **2014**, *3*, 63–77. [CrossRef]
46. Zoungrana, B.J.; Conrad, C.; Amekudzi, L.; Thiel, M.; Da, E.; Forkuor, G.; Löw, F. Multi-Temporal Landsat Images and Ancillary Data for Land Use/Cover Change (LULCC) Detection in the Southwest of Burkina Faso, West Africa. *Remote Sens.* **2015**, *7*, 12076–12102. [CrossRef]
47. Son, J.; Jung, I.; Park, K.; Han, B. Tracking-by-segmentation with online gradient boosting decision tree. In Proceedings of the 2015 IEEE International Conference on Computer Vision (ICCV), Santiago, Chile, 7–13 December 2015; pp. 3056–3064. [CrossRef]
48. Naboureh, A.; Ebrahimy, H.; Azadbakht, M.; Bian, J.; Amani, M. Ruesvms: An ensemble method to handle the class imbalance problem in land cover mapping using google earth engine. *Remote Sens.* **2020**, *12*, 3484. [CrossRef]
49. Mas, J.-F.; Pérez-Vega, A.; Ghilardi, A.; Martínez, S.; Loya-Carrillo, J.O.; Vega, E. A Suite of Tools for Assessing Thematic Map Accuracy. *Geogr. J.* **2014**, *2014*, 372349. [CrossRef]
50. Loosvelt, L.; Peters, J.; Skriver, H.; Lievens, H.; Van Coillie, F.M.B.; De Baets, B.; Verhoest, N.E.C. Random Forests as a tool for estimating uncertainty at pixel-level in SAR image classification. *Int. J. Appl. Earth Obs. Geoinf.* **2012**, *19*, 173–184. [CrossRef]
51. Pontius, R.G.; Gao, Y.; Giner, N.M.; Kohyama, T.; Osaki, M.; Hirose, K. Design and Interpretation of Intensity Analysis Illustrated by Land Change in Central Kalimantan, Indonesia. *Land* **2013**, *2*, 351–369. [CrossRef]
52. Aldwaik, S.Z.; Pontius, R.G. Intensity analysis to unify measurements of size and stationarity of land changes by interval, category, and transition. *Landsc. Urban Plan.* **2012**, *106*, 103–114. [CrossRef]
53. Exavier, R.; Zeilhofer, P. OpenLand: Software for Quantitative Analysis and Visualization of Land Use and Cover Change. *R J.* **2020**, *12*, 359–371. [CrossRef]
54. Al Kafy, A.; Al-Faisal, A.; Mahmudul Hasan, M.; Sikdar, M.S.; Hasan Khan, M.H.; Rahman, M.; Islam, R. Impact of LULC Changes on LST in Rajshahi District of Bangladesh: A Remote Sensing Approach. *J. Geogr. Stud.* **2019**, *3*, 11–23. [CrossRef]
55. Bhat, P.A.; ul Shafiq, M.; Mir, A.A.; Ahmed, P. Urban sprawl and its impact on landuse/land cover dynamics of Dehradun City, India. *Int. J. Sustain. Built Environ.* **2017**, *6*, 513–521. [CrossRef]
56. Boyer, F.; Delaunay, D. « *OUAGA. 2009 » Peuplement de Ouagadougou et Développement Urbain Rapport Provisoire*; Ambassade de France: Ouagadougou, Burkina Faso, 2009.
57. Niya, A.K.; Huang, J.; Karimi, H.; Keshtkar, H.; Naimi, B. Use of intensity analysis to characterize land use/cover change in the biggest Island of Persian Gulf, Qeshm Island, Iran. *Sustainability* **2019**, *11*, 4396. [CrossRef]
58. Gogoi, P.P.; Vinoj, V.; Swain, D.; Roberts, G.; Dash, J.; Tripathy, S. Land use and land cover change effect on surface temperature over Eastern India. *Sci. Rep.* **2019**, *9*, 8859. [CrossRef]
59. Turok, I.; McGranahan, G. Urbanization and economic growth: The arguments and evidence for Africa and Asia. *Environ. Urban.* **2013**, *25*, 465–482. [CrossRef]
60. World Bank. *Burkina Faso: Upgrading of Low Income Settlements Country Assessment Report*; World Bank: Washington, DC, USA, 2002.